

Cellular Automata for Medical Image Processing

Sartra Wongthanavas
 Khon Kaen University
 Thailand

1. Introduction

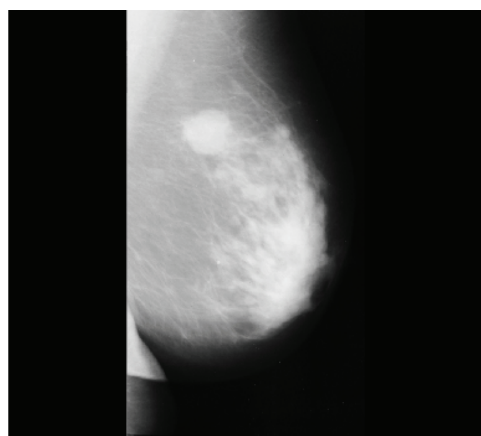
Cellular automata (CA) were introduced to provide a formal framework for investigating the behaviour of dynamic complex system in which time and space are discrete. They comprise an array of cells, where each cell can be in one of a finite number of possible states, which is updated synchronously in discrete time steps according to local transition rules (cell rules). A state of a cell at the next time step is determined by its neighboring cell's current state. A substantial numbers of CA activities occurred in the 1970s with the introduction of artificial life. There were a number of distinguished papers and books to date has investigated artificial life (Raghawan, 1993; Langton, 1986, 1992; Pesavento, 1995; Rietman, 1993). Interest in important features of physics was spawned largely by Tommaso Toffoli. Stephen Wolfram was responsible for capturing the wider interest of the physics community with a series of papers in the 1980s, while others were applying CAs to a variety of problems in other fields (Sarkar & Abbasi, 2006; Xiao et al., 2008; Bandini et al., 2001; Mizas et al., 2008). In present, CA are being studied from many widely different angles, and the relationship of these structures to existing problems in being constantly sought and discovered (Reynaga & Amthauer, 2003; Mitchell et al., 1994; Hecker et al., 1999). As the topology of CA, they appear as natural tools for image processing due to their local nature and simple parallel computation implementation. To date, there are a number of papers which generally discuss cellular automata for image processing (Hernandez & Herrmann, 1996; Rosin, 2006; Chen & Horng, 2010; Chen & Lai, 2007; Eslami et al., 2010; Tzionas et al., 1997; Umeo, 2001). In this regard, there were some papers discuss medical image processing using CA model (Cheng et al, 2006; Viher et al, 1998, Ferrari et al., 2004; Chen et al., 2008). This paper presents a number of cellular automata-based algorithms for medical image processing. It starts by introducing cellular automata fundamentals necessary for understanding the proposed algorithms. Then, a number of cellular automata algorithms for medical image edge detection, noise filtering, spot detection, pectoral muscle identification and segmentation was presented. In this regard, 2-D mammogram images for the breast cancer diagnosis were investigated.

2. Cellular automata

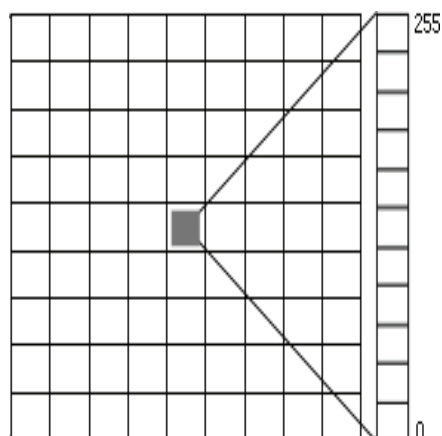
Let I denote the set of integer. A 2-D cellular space is a 4-tuple, $(I \times I, V, N, f)$, where $I \times I$ is a set of cartesian product of two integer sets, V is a set of cellular states, N is the type of neighborhood, and f is the local transition function from V^n into V . The relevant neighborhood function is a function from $I \times I$ into $2^{I \times I}$ defined by $g(\alpha) = \{\alpha + \delta_1, \alpha + \delta_2, \dots,$

$\alpha + \delta_n$ }, for all $\alpha \in I \times I$, where δ_i ($i = 1, 2, \dots, n$) $\in I \times I$ is fixed. The neighborhood state function of a cell α at time t is defined by $h^t(\alpha) = (v^t(\alpha + \delta_1), v^t(\alpha + \delta_2), \dots, v^t(\alpha + \delta_n))$. For 2-D von Neumann neighborhood, the neighborhood state function of the central cell (α) is defined by: $h^t(\alpha) = (v^t(\alpha + (0,0)), v^t(\alpha + (0,1)), v^t(\alpha + (1,0)), v^t(\alpha + (0,-1)), v^t(\alpha + (-1,0)))$, where $v^t(\alpha + (0,0))$ is current state of the central cell, $v^t(\alpha + (0,1))$ ($v^t(\alpha + (0,-1))$) for the north (south) cells, $v^t(\alpha + (1,0))$ ($v^t(\alpha + (-1,0))$) for the east (west) cells.

Now we relate the neighborhood state of a cell α at time t to the cellular state of that cell at time $t+1$ by $f(h^t(\alpha)) = v^{t+1}(\alpha)$. The function f is referred to as the 2-D CA rule and is usually given in the form of a state table, specifying all possible pairs of the form $(h^t(\alpha), v^{t+1}(\alpha))$. Figure 1 shows 2-D digital image and 2-D CA.



(a) 2-D digital image.



(b) 2-D cellular automata with 256 states.

Fig. 1. A 2-D digital image vs A 2-D CA.

3. Cellular automata for medical image edge detection

As stated previously, cellular automata techniques appear as a natural tool for image processing due to their local nature and simple parallel computing implementation. This section presents one main algorithm and investigates its variation for processing mammogram images. The algorithms will cope with edge detection and noise removal for both binary and grayscale images, while the last one will correspond to hypothesized spots detection for breast cancer analysis. Examples of the application of these cellular automata techniques to real mammogram images will be presented, which together with the results will show the performance characteristics.

The main cellular automata algorithm for k gray levels of digital images is on the basis of a two dimensional cellular automata $(I \times I, V, N, f)$ with $V = \{0, 1, 2, \dots, k-1\}$, where k is a number of states, N is the type of neighborhood, while the local transition function f is from V^n into V . The proposed algorithm is shown in (1) below:

$$f((v^t(\alpha + \delta_1), v^t(\alpha + \delta_2), \dots, v^t(\alpha + \delta_n))) = E(\alpha), \quad \text{if } \max_{j=0}^{k-1} N(C_j) = C_{\text{target}} \text{ and } \text{sum}(v^t(C_{\text{target}})) > k-1 \quad (1)$$

$$= B(\alpha), \quad \text{otherwise}$$

where C_j is the j^{th} class of the pixel values (states) in its neighborhood ($h^t(\alpha)$) for $j = 0, 1, 2, \dots, m$ and $v^t(\alpha + \delta_i) \in C_j$.

$N(C_j)$ is a number of neighbors of α which fall into class C_j .

$\text{sum}(v^t(C_{\text{target}}))$ is summation of $v^t(C_{\text{target}})$.

C_{target} is the majority class containing maximal number of neighbors.

$v^t(C_{\text{target}})$ denotes all of $v^t(\alpha + \delta_i) \in C_{\text{target}}$.

$E(\alpha)$ is the edge pixel value.

$B(\alpha)$ is the background pixel value.

k is a number of states.

For class arrangement, histogram distribution will be utilized to supervise an identification of each class. Automatic class arrangement can be implemented using Otsu algorithm (Otsu, 1979).

3.1 Grayscale images

The objective of the edge detection techniques is to enhance the magnitude of the local differences in gray level values between regions of the images. Over regions which are different, changes must be made to enhance the edges. The proposed variation of (1) which deals with this task is shown in formula (2) for Von Neumann's neighborhood, four classes and 256 gray levels as following:

$$f((v^t(\alpha + \delta_1), v^t(\alpha + \delta_2), \dots, v^t(\alpha + \delta_5))) = 255, \quad \text{if } \max_{j=0}^3 N(C_j) = C_{\text{target}} \text{ and } \text{sum}(v^t(C_{\text{target}})) > 255 \quad (2)$$

$$= 0, \quad \text{otherwise}$$

where C_j is the j^{th} class of the pixel values in its neighborhood ($h^t(\alpha)$) for $j = 0, 1, 2, 3$ and $v^t(\alpha + \delta_i) \in C_j$.

$N(C_j)$ is number of neighbors of α which fall into class C_j .

C_{target} is the majority class containing maximal number of neighbors ($v^t(\alpha + \delta_i) \in C_{\text{target}}$).

$\text{sum}(v^t(C_{\text{target}}))$ is summation of $v^t(C_{\text{target}})$.

$v^t(C_{\text{target}})$ denotes all of $v^t(\alpha + \delta_i) \in C_{\text{target}}$.

Prior to implementing the formula (2) on a particular image, a class arrangement using histogram information was determined. Figure 2 shows an original mammogram image (a) and its histogram information (b). Results for four classes arrangement and the edge image were shown in Figure 2 (c) and (d), respectively.

It is explicitly shown that the cellular automata algorithm simply provides the promising edge maps shown in Fig. 3(d).

3.2 Binary images

In case of edge detection on binary mammogram, the cellular automata algorithm given in the formula (2) directly enables carrying out to two states efficiently. There is no need to be changed. Figure 3 shows the promising result implementing the algorithm. An Edge result exhibits the superb quality with one pixel wide and edge has no break.

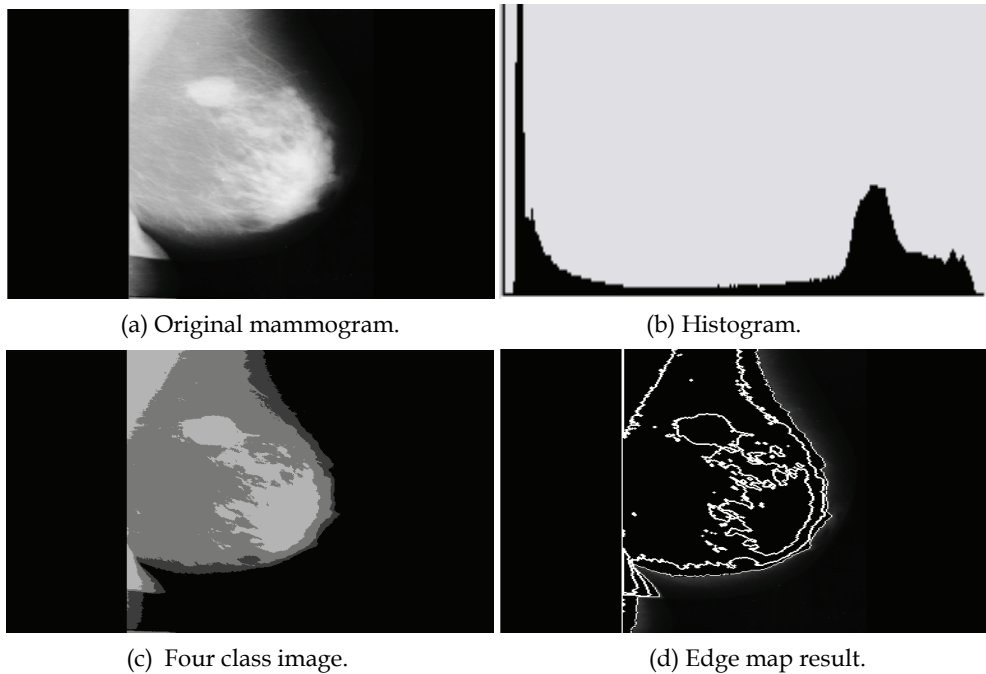


Fig. 2. (a) Original mammogram, (b) histogram information, (c) four classes of image, and (d) result of edge detection.

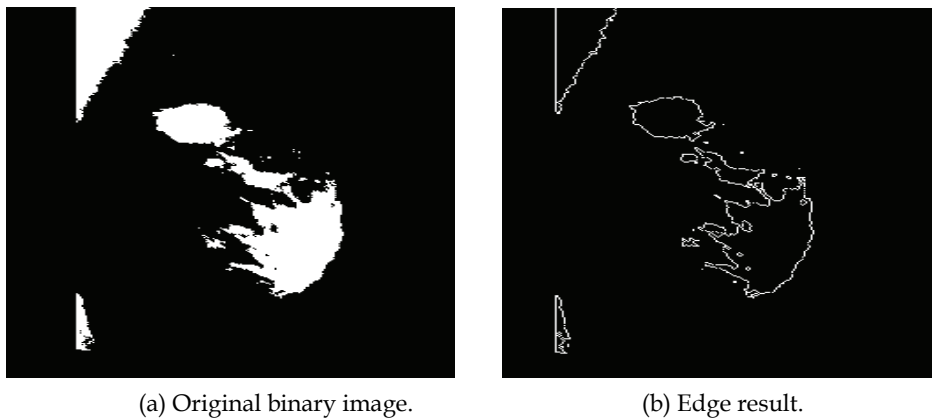


Fig. 3. Edge result as dealing with binary image.

3.3 Noise filtering

The objective of the noise filtering is to reduce the local differences in gray level values between regions of the images. Over regions which are similar, no changes must be made, in order to avoid the destruction of the main characteristics of the image. The proposed

variation of cellular automata algorithm given in (1) using von Neumann’s neighborhood and two states dealing with this task is shown in formula (3) as follow:

$$f((v^t(\alpha + \delta_1), v^t(\alpha + \delta_2), \dots, v^t(\alpha + \delta_5))) = \begin{cases} \max(v^t(C_{target})), & \text{if } \max_{j=0}^3 N(C_j) = C_{target} \\ 0, & \text{otherwise} \end{cases} \quad (3)$$

where C_j is the j^{th} class of the pixel values in its neighborhood ($h^t(\alpha)$) for $j = 0, 1, 2, 3$ and $v^t(\alpha + \delta_i) \in C_j$.

$N(C_j)$ is number of neighbors of α which fall into class C_j .

C_{target} is the majority class containing maximal number of neighbors ($v^t(\alpha + \delta_i) \in C_{target}$).

$v^t(C_{target})$ denotes all of $v^t(\alpha + \delta_i) \in C_{target}$.

$\max(v^t(C_{target}))$ is the maximal state of $v^t(C_{target})$.

Figure 4 shows an original binary mammogram with 2% salt and pepper noise. The noise filtering result obtained by implementing the algorithm (3) using one step of iteration was shown in Figure 4 (b). In this respect, the cellular automata algorithm (3) explicitly provides the promising result.



(a) Noisy binary image.

(b) Noise removal.

Fig. 4. Binary image with 2% salt and pepper noise (a) and the image after noise removal (b).

3.4 Spot detection

The objective of the spot detection is to assist the physicians and doctors in locating hypothesized spots for masses in breast cancer. The shape and spread region of spots play a vital role for further steps of analyses and have to be comprehensively taken into account. For this purpose, a set operator is implemented as follow:

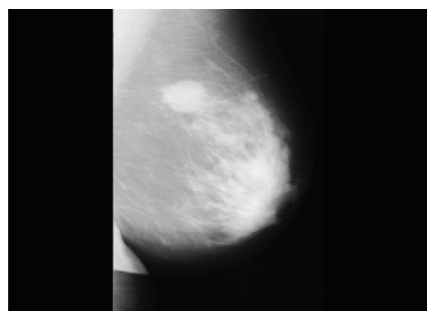
$$W = X - Y \quad (4)$$

where X denotes an investigating original image,

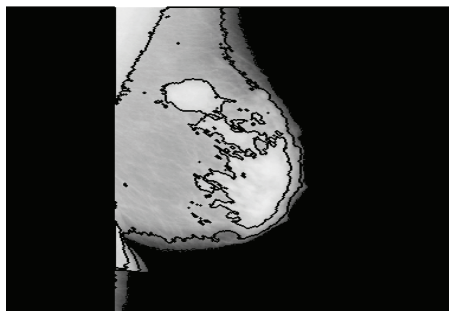
Y denotes an edge map resulting from implementing the formula (2), and

W denotes the spot detection image.

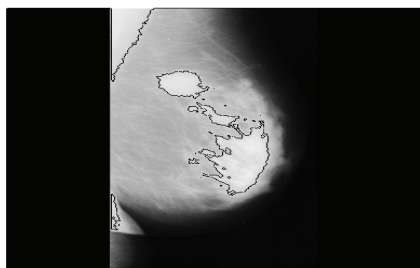
The operator (-) represents the subtraction, meaning that it simply carries out the subtraction of pixel values in the same coordinate between two images (sets). By implementing such an operator in an original image (X) shown in Fig. 5(a) with respect to the edge image Y obtained by implementing the formula (2) on grayscale and binary images, the resulting spot detection was shown in Figure 5 (b) and (c), respectively.



(a) Malignant mammogram



(b) Spot detection using grayscale image.



(c) Spot detection using binary image.

Fig. 5. Spot detection due to (2) for binary and grayscale images.

Figure 5. shows mammogram processing with white spot detection: (a) original malignant mass in mammogram, (b) hypothesized mass detection using algorithm (2) for grayscale, and (c) hypothesized mass detection using algorithm (3) for binary image.

4. Cellular automata for identification of the pectorial muscle in mammograms

The pectoral muscle represents a predominant density region in most medio-lateral oblique (MLO) views of mammograms. Its inclusion can affect the results of intensity-based image processing methods. To date, there were some papers has investigated identification of the pectoral muscle in mammograms (Ferrari et al., 2004; Ma et al., 2007). This section presents a new method on the basis of cellular automata model for the identification of the pectoral muscle in MLO mammograms. A dataset of 84 MLO mammograms from the MIAS (Mammographic Image Analysis Society, London, U.K.) database (Suckling et al., 1994) was implemented throughout for evaluation. In this respect, the pectoral muscle edge detected in the mammograms was carried out based upon the percentage of false-positive (FP) and false-negative (FN) pixels determined by comparison between the numbers of pixels enclosed in the regions delimited by the edges identified by a radiologist and by the proposed method.

4.1 Proposed CA-based algorithm

In this section, the method for identification of pectoral muscle in mammogram images were presented. It starts by computing the edge detection by using the formula (2) stated earlier dealing with grayscale images. Then, the result will be segmented by using the rule-based

algorithm, leading to the identification of the pectoral muscle. Examples of the application of the proposed method to real mammogram images will be presented, which together with the results will show the performance characteristics.

The proposed cellular automata algorithm for 256 gray levels of digital images are on the basis of a two-dimensional cellular automata $(I \times I, V, N, f)$ with $V = \{0, 1, 2, \dots, 255\}$, N is von Neumann type of the neighborhood, while the local transition function f is from V^n into V .

4.1.1 Edge detection

Referred to the formula (2) stated previously, the cellular automata algorithm for this task was revisited as follow:

$$v^t(\alpha + \delta_i), v^t(\alpha + \delta_2), \dots, v^t(\alpha + \delta_5) = 255, \quad \text{if } \max_{j=0}^3 N(C_j) = C_{\text{target}} \text{ and } \text{sum}(v^t(C_{\text{target}})) > 255$$

$$= 0, \quad \text{otherwise}$$

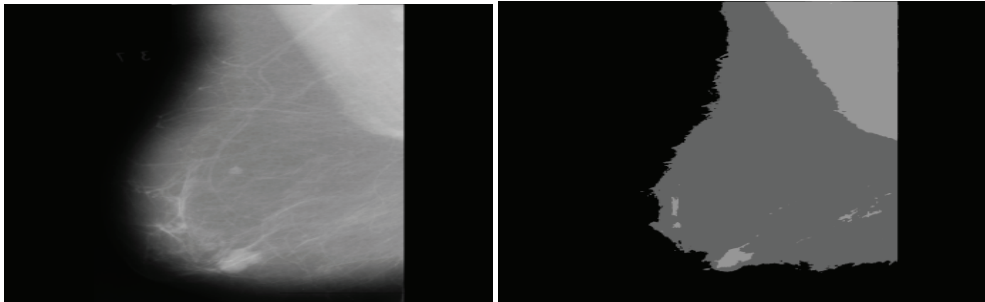
where C_j is the j^{th} class of the pixel values in its neighborhood $(h^t(\alpha))$ for $j = 0, 1, 2, 3$ and $v^t(\alpha + \delta_i) \in C_j$.

$N(C_j)$ is number of neighbors of α which fall into class C_j .

C_{target} is the majority class containing maximal number of neighbors $(v^t(\alpha + \delta_i) \in C_{\text{target}})$.

$\text{sum}(v^t(C_{\text{target}}))$ is summation of $v^t(C_{\text{target}})$.

$v^t(C_{\text{target}})$ denotes all of $v^t(\alpha + \delta_i) \in C_{\text{target}}$.



(a) Original image mdb005.

(b) Four class image.

(c) Edged image.

Fig. 6. Results obtained for the image mdb005: (a) Original image, (b) Its four class image, and (c) Edged image obtained by implementing (2).

Prior to implementing the algorithm (2), an original mammogram image of mdb005 (Suckling et al., 1994) was classified into four classes (C_j) due to Otsu algorithm (Otsu, 1979). The results were shown in Figure 6.

4.1.2 Pectoral muscle identification

As already mentioned, the inclusion of pectoral muscle in mammogram can affect the results of intensity-based image processing methods or bias procedures in the detection of breast cancer. The objective of the pectoral muscle identification is to determine the pectoral muscle for the exclusion from the mammograms prior to process in further steps for breast cancer diagnosis. In this regard, the edge resulting image was used in the segmentation algorithm given as follow:

Algorithm: 1 Pectoral muscle identification

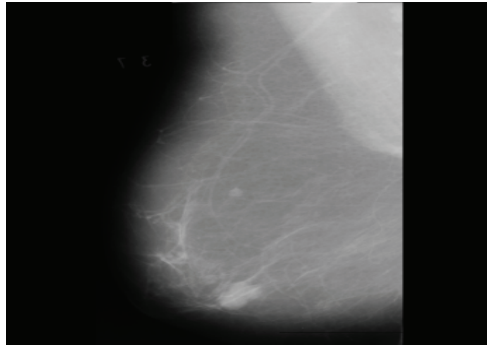
Step 1: Removal of unqualified objects.

1. Implement the formula (2) in a mammogram image P, resulting in the image Q.
2. Filter unqualified objects, objects consisting of contiguous edge less than 2,500 pixels, out of the Q resulting in the image R.

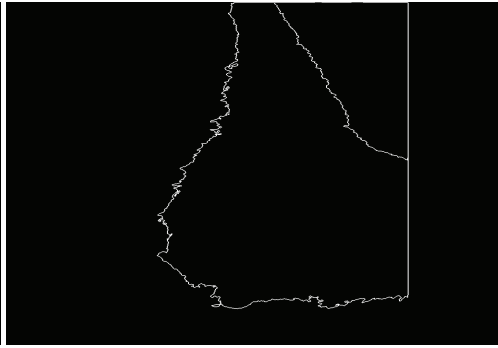
Step 2: Identification of pectoral muscle.

1. FOR i:= 1 TO n DO
Find the area of ROI_r(i).
{ ROI_r(i) is a region of interest i inside the image R. ROI_r at region i is the i-th area surrounded by an edge boundary on image R.}
2. Pectoral muscle segmentation:
 - 2.1 MUSCLE := NIL {empty set}
 - 2.2 FOR j:=1 TO n DO
IF ROI_r(j) > max_size AND ROI_r(j) ≤ min_size
THEN ROI_r(j) := background
{ Set the ROI_r(j) to background when it is not of interest regions. In practical uses in our implementation, max_size = 95,200 pixels, and min_size = 2,500 pixels.}
 - ELSE IF min(y, ROI_r(j)) > min_upper
THEN ROI_r(j) := background
{ min(y, ROI_r(j)) denotes minimal value of y for a coordinate (x,y) of any pixels in the region of ROI_r(j). In our implementation, min_upper = 60.}
{ Regions of interest will locate at min(y, ROI_r(j)) in which is at the topmost part of the image R. }
 - ELSE IF mean(y, ROI_r(j)) > min_y_average
THEN ROI_r(j) := background
{ mean(y, ROI_r(j)) is an average of y for coordinates (x,y) inside the region of ROI_r(j)
In our implementation, min_y_average = 350. }
 - ELSE IF mean(I, ROI_r(j)) > min_average_intensity
THEN MUSCLE := MUSCLE ∪ ROI_r(j)
{ mean(I, ROI_r(j)) is an average intensity of all pixels inside the region of ROI_r(j).
In our implementation, min_average_intensity = 157. }

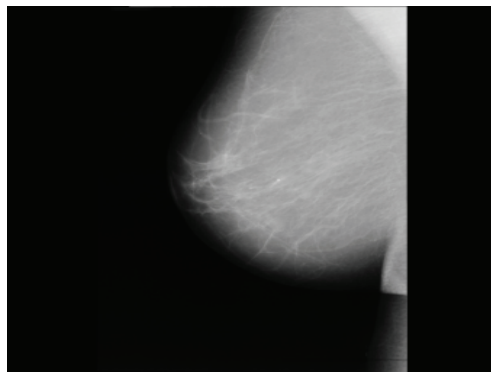
The results in implementing the proposed segmentation algorithm on mdb005 and mdb011 were shown in Fig. 7. Fig. 8 shows hand-drawn pectoral muscle edge by radiologist as applied to mdb005, the result obtained by the proposed algorithm, and the pectoral muscle removal according to the proposed algorithm.



(a) Original image mdb005.



(b) Result obtained by the algorithm 2.



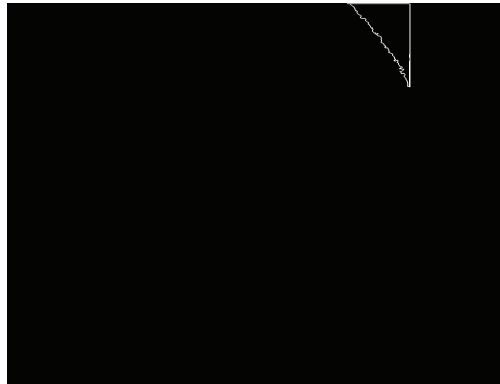
(c) Original image mdb011.



(d) Result obtained by the algorithm 2.

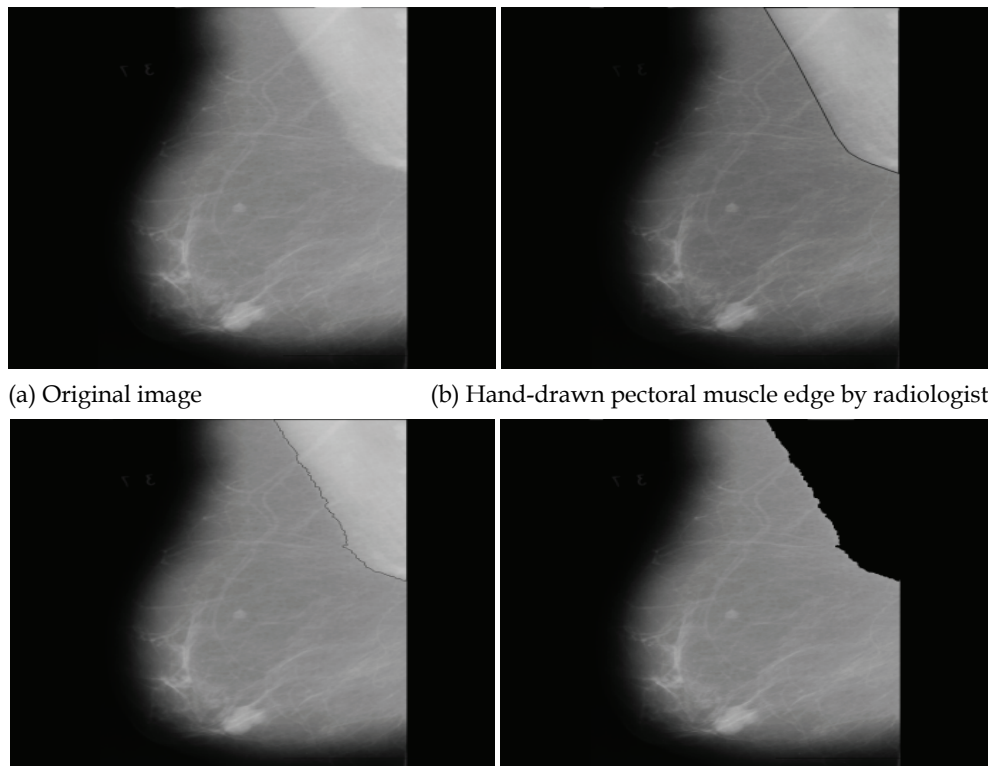


(e) Pectoral muscle identification of mdb005.



(f) Pectoral muscle identification of mdb011.

Fig. 7. Results obtained from proposed algorithm: (a) and (c) are original images mdb005 and mdb011, respectively, (b) and (d) are edge results due to original images (a) and (c), respectively, and (e) and (f) are results obtained from the pectoral muscle identification algorithm due to original images (a) and (c), respectively.



(a) Original image

(b) Hand-drawn pectoral muscle edge by radiologist

(c) Pectoral muscle edges detected by the algorithm. (d) Pectoral muscle removal using the algorithm.

Fig. 8. Results obtained for the image mdb005: (a) original image, (b) hand-drawn pectoral muscle edge by radiologist superimposed on the original image, (c) pectoral muscle edges detected by the CA-based method superimposed on the original image, and (d) pectoral muscle removal using the CA-based method.

4.2 Performance evaluation and results

For performance evaluation purpose, the total of 84 images, randomly selected from the Mammographic Image Analysis Society, London, U.K. (Suckling et al., 1994), were used in experimentation. The spatial resolution of these images is $200\ \mu\text{m}$ and depth resolution in 8 bit. The images in the database are 1024×1024 pixels in size. The result obtained from the proposed method was evaluated in consultation with radiologists experienced in mammography. Then, the pectoral muscle edges were manually drawn by the author under the supervision of radiologists, without referring to the results of detection by the proposed method. The segmentation results of the proposed method was evaluated based upon the number of false-positive (FP) and false-negative (FN) pixels in the regions demarcated by the manually drawn edges. An FP pixels was defined as a pixel outside the reference region that was included in the pectoral region segmented. An FN pixel was defined as a pixel in the reference region that was not present within the segmented region. Table 1 shows mean

and standard deviation values of the FP and FN pixels for the result of the proposed method with 84 images.

CA-based algorithm	Statistics
Analysis of area enclosed	
FP $\pm \sigma$	1.99 \pm 8.19%
FN $\pm \sigma$	18.89 \pm 14.19%
# images with (FP and FN) < 5%	13
# images with 5% <(FP and FN) <10%	15
# images with (FP and FN) > 10%	56

Table 1. Mean and standard deviation values of the FP and FN pixels for the results of CA-based algorithm with 84 images.

Table 1 shows an interesting statistical results that the identification obtained by the CA-based algorithm provides the promising results with minimal FP and FN. In this regard, the proposed CA-based algorithm is one of promising methods in pectoral muscle identification for mammogram processing.

5. Cellular automata for mass segmentation in mammograms

This section investigates algorithms on the basis of cellular automata model for coping with the segmentation of hypothesized masses in mammograms. The 256-states cellular automata algorithms were developed to deal with 256 grayscale mammogram images for determining masses. The proposed cellular automata algorithms investigated here are on the basis of two dimensional CAs (IxL, V, N, f) with $V = \{0, 1, 2, \dots, 255\}$, Von Neumann's neighborhood N, while the local transition function f is from V_n into V. The results will be used for determining mass features in breast cancer diagnosis. An empirical experimentation shows that the proposed cellular automata algorithms provide the superior results.

The proposed segmentation algorithm utilizes a concept of two-types bacteria propagation. The first type confiscates a mass seed, which is an object image, while the second one confiscates the background which is declared by a circle surrounding the mass seed. Both types of bacteria propagate to their neighbors in parallel at each time step depending on its and their neighbor's strengths. A circle surrounding a mass seed shown in Fig. 4 (a) represents the background seed being seized by the other type of bacteria. Both types of bacteria continue propagating in parallel in discrete time steps as stated earlier. In order to reduce the computation time, the proposed algorithm can be stopped anytime earlier so far as the propagation of bacteria taken up the mass seed is consistent. The CA-based segmentation algorithm is given as follow:

Algorithm: 2 CA-based algorithm for mass segmentation

```
// Identify hypothesized mass seed from a mammogram image P; mark the mass seed
// Identify object seed from a mammogram image P; mark the object seed
// For each cell (pixel) in P
  for  $\forall p \in P$ 
    // copy previous state
       $l_p^{t+1} = l_p^t;$ 
```

```

 $\theta_p^{t+1} = \theta_p^t;$ 
// neighbors try to attack current cell
for  $\forall q \in N(p)$ 
    if  $g(\|C_p - C_q\|_2) \cdot \theta_q^t > \theta_p^t$  then
         $l_p^{t+1} = l_q^t;$ 
         $\theta_p^{t+1} = g(\|C_p - C_q\|_2) \cdot \theta_q^t$ 
    end if
end for
end for

```

where P denotes an image, p denotes a pixel.

θ_q^t denotes the strength of a cell $q \in Q$ at time t .

θ_p^t denotes the strength of a p 's neighboring cells at time t .

l_p^t, l_p^{t+1} denote the centering cell state of p at time t and $t+1$, respectively.

l_q^t, l_q^{t+1} denote the neighboring cell state of q at time t and $t+1$, respectively.

$N(p)$ denotes neighboring cells of p .

$\|C_p - C_q\|_2$ denotes the Euclidian distance between a cell q and a neighboring cell p .

$g(x)$ represents a monotonous decreasing function defined by (2) as following

$$g(x) = 1 - \frac{x}{\max\|C\|_2} \quad (5)$$

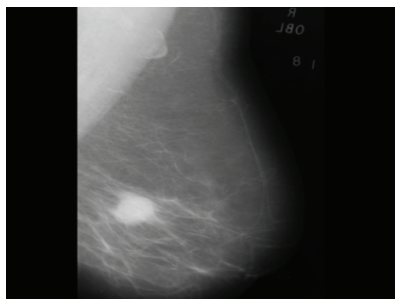
In implementing the algorithm 2, the termination condition was satisfied if the configuration of mass seed has not been changed, meaning that their states were steady. This abundantly reduces time complexity in practical implementation. Figure 9 shows the results of implementing the proposed mass segmentation algorithm on the mammogram mdb028. The hypothesized mass seeds, depicted by red shadow, and background seeds, depicted by blue circle, are represented two types of bacteria as shown in in Fig. 8 (a) and (b), respectively. Fig. 8 (c) and (d) show a series of propagating results on the 40 evolution steps and the final result at iteration 72. Fig. 10 shows the results of mass segmentation of mdb005 and mdb092 superimposed on the original mammograms, respectively.

6. Conclusions and discussions

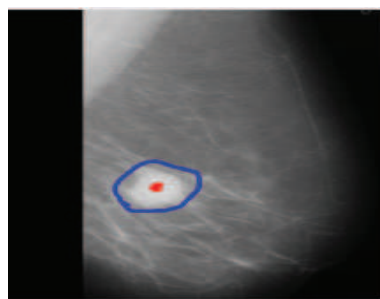
The behavior of cellular automata is fascinating not only from theory but also from applications. They offer the beauty and elegance of results in medical image processing as reported in literature. In this work we have presented a number of uniform cellular automata algorithms for mammogram image processing. Based on empirical experimentation, the proposed algorithms give the promising results when tested on MIAS mammograms. This quite encourages in determining other tasks for the research. In this regard, we have more investigations on applications for mammogram and other medical image processing and hope report in the near future.

7. Acknowledgement

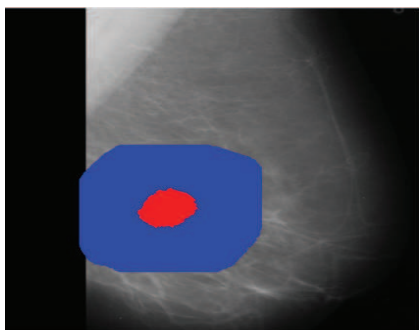
We deeply thank to The Thailand Research Funds (TRF) for financial support of the research project due to RMU5080010.



(a) Original image mdb028.



(b) Seeds of object and background.



(c) Evolution result at 40 time steps

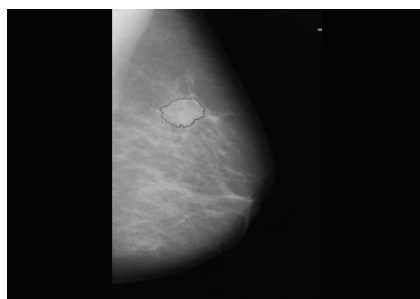


(d) Result at final time steps (72)

Fig. 9. Mass segmentation results obtained from the image mdb028: (a) original image, (b) initial seeds, (c) result after 40 time steps of evolution, and (d) final result at iteration 72.



(a) Mass segmentation result of mdb005.



(b) Mass segmentation result of mdb092.

Fig. 10. Mass segmentation obtained from the image mdb005 and mdb092: (a) mass segmentation result of mdb005 superimposed on the original mammogram, and (b) mass segmentation result of mdb092 superimposed on the original mammogram.

8. References

- Hernandez, G. & Herrmann, J. (1996). Cellular Automata for Elementary Image Enhancement. *Graphical Models and Image Processing (GMIP)*, Vol. 4, No. 58, pp. 82-89.
- Wongthanavas, S. & Lursinsap, C. (2004). A 3-D CA-based Edge Operator for 3-D Images, *Proceedings of ICIP 2004 11th International Conference on Image Processing*, pp. 235-238, ISBN 0-7803-8555-1, Singapore, October 24-27, 2004.
- Rosin, P. (2006). Training Cellular Automata for Image Processing. *IEEE Transactions on Image Processing*, Vol. 15, No. 7, pp. 2076-2087.
- Cheng, H. D., Shi, X.J., Min, R., Hu, L.M., Cai, X.P. & Du, H.N. (2006). Approaches for Automated Detection and Classification of Masses in Mammograms. *Pattern Recognition*, Vol. 39, pp. 646-668.
- Viher, B., Dobnikar, A. & Zazula, D. (1998). Cellular Automata and Follicle Recognition Problem and Possibilities of Using Cellular Automata for Image Recognition Purposes. *International Journal of Medical Informatics*, Vol. 49, pp. 231-241.
- Ferrari, R.J., Rangayyan, R.M., Desautels, J.E., Borges, R.A. & Frere, A.F. (2004). Automatic Identification of the Pectoral Muscle in Mammograms. *IEEE Transactions on Medical Imaging*, Vol. 23, No. 2, pp. 232-245.
- Otsu, N. (1979). A Threshold Selection Method from Gray-level Histograms. *IEEE Transactions on Systems Man Cybernetics*, Vol. 9, No. 1, pp. 62-66.
- Suckling, J., Parker, J., Dance, D., Astley, S., Hutt, I, Boggis, C., Ricketts, I., Stamatakis, E., Cerneaz, N., Kok, S., Taylor, P., Betal, D. & Savage, J. (1994). The mammographic images analysis society digital mammogram database, *Exerpta Medica. International Congress Series 1069*, pp. 375-378
- Ma, F., Slavotinek, J. & Bottema, M.J. (2007). Two graph theory based methods for identifying the pectoral muscle in mammograms. *Pattern Recognition*, Vol. 40, pp. 2598-2598
- Wongthanavas, S. & Tangvoraphongchai, V. (2007). CA-based Algorithms and Its Application in Medical Image Processing. *Proceedings of ICIP 2007 14th International Conference on Image Processing*, pp. III-41-44, ISBN: 1-4244-1437-7, ISSN: 1522-4880, San Antonio, Texas, U.S.A. September 16-19, 2007.
- Wongthanavas, S. & Tangvoraphongchai, V. (2008). Cellular Automata-based Identification of The Pectoral Muscle in Mammograms. *Proceedings of ISBME 2008 3rd International Symposium on Biomedical Engineering*, pp. 294-298, November 10-11, 2008, Bangkok, Thailand, November 10-11, 2008.
- Chen, R.J. & Lai, L.L. (2007). Image security system using recursive cellular automata substitution. *Pattern Recognition*, Vol. 40, No. 5, May 2007, pp. 1621-1631
- Chen, R.J. & Horng, S.J. (2010). Novel SCAN-CA-based image security system using SCAN and 2-D von Neumann cellular automata. *Signal Processing: Image Communication*, Vol. 25, Issue 6, July 2010, pp. 413-426
- Reynaga, R. & Amthauer, E. (2003). Two-dimensional cellular automata of radius one for density classification task, *Pattern Recognition Letters*, Vol. 24, Issue 15, November 2003, pp. 2849-2856

- Mitchell, M., Crutchfield, J.P & Hraber, P.T. (1994). Evolving cellular automata to perform computations: mechanisms and impediments. *Physica D: Nonlinear Phenomena*, Vol. 75, Issues 1-3, 1 August 1994, pp. 361-391
- Wongthanavas, S. & Sadananda, R. (2003). A CA-based edge operator and its performance evaluation. *Journal of Visual Communication and Image Representation*, Vol. 14, Issue 2, June 2003, pp. 83-96
- Rogowska, J. (1999). Overview and Fundamentals of Medical Image Segmentation. *Handbook of Medical Image Processing and Analysis (Second Edition)*, pp. 73-90
- Hecker, C., Roytenberg, D., Sack, J.R. & Wang, Z. (1999). System development for parallel cellular automata and its applications. *Future Generation Computer Systems*, Vol. 16, Issues 2-3, December 1999, pp. 235-247
- Karafyllidis, I. (1999). Acceleration of cellular automata algorithms using genetic algorithms. *Advances in Engineering Software*, Vol. 30, Issue 6, June 1999, pp. 419-437
- Sarkar, C. & Abbasi, S.A. (2006). Cellular automata-based forecasting of the impact of accidental fire and toxic dispersion in process industries. *Journal of Hazardous Materials*, Vol. 137, Issue 1, 1 September 2006, pp. 8-30
- Xiao, X., Wang, P. & Chou, K.-C. (2008). Predicting protein structural classes with pseudo amino acid composition: An approach using geometric moments of cellular automaton image. *Journal of Theoretical Biology*, Vol. 254, Issue 3, 7 October 2008, pp. 691-696
- Eslami, Z., Razzaghi, S.H. & Ahmadabadi, J.Z. (2010). Secret image sharing based on cellular automata and steganography. *Pattern Recognition*, Vol. 43, Issue 1, January 2010, pp. 397-404
- Tzionas, P., Thanailakis, A. & Tsalides, P. (1997). An efficient algorithm for the largest empty figure problem based on a 2D cellular automaton architecture. *Image and Vision Computing*, Vol. 15, Issue 1, January 1997, pp. 35-45
- Umeo, H. (2001). Linear-time recognition of connectivity of binary images on 1-bit inter-cell communication cellular automaton. *Parallel Computing*, Vol. 27, Issue 5, April 2001, pp. 587-599
- Bandini, S., Mauri, G. & Serra, R. (2001). Cellular automata: From a theoretical parallel computational model to its application to complex systems. *Parallel Computing*, Vol. 27, Issue 5, April 2001, pp. 539-553
- Chen, J.-C., Yeh, C.-M. & Tzeng, J.-E. (2008). Pattern differentiation of glandular cancerous cells and normal cells with cellular automata and evolutionary learning. *Expert Systems with Applications*, Vol. 34, Issue 1, January 2008, pp. 337-346
- Mizas, C., Sirakoulis, G.C., Mardiris, V., Karafyllidis, I., Glykos, N. & Sandaltzopoulos R. (2008). Reconstruction of DNA sequences using genetic algorithms and cellular automata: Towards mutation prediction?. *Biosystems*, Vol. 92, Issue 1, April 2008, pp. 61-68
- Richards, F.C., Meyer, T.P. & Packard, N.H. (1990). Extracting cellular automaton rules directly from experimental data. *Physica D: Nonlinear Phenomena*, Vol. 45, Issues 1-3, 2 September 1990, pp. 189-202
- Raghavan, R. (1993). Cellular automata in pattern recognition. *Information Sciences*, Vol. 70, Issues 1-2, May 1993, pp. 145-177

- Langton, C.G. (1986). Studying artificial life with cellular automata. *Physica D*, Vol. 22, pp. 120-140
- Langton, C.G. (1992). Life at the edge of chaos. *Artificial life*, Vol. 2, No. 4, pp 41-91
- Pesavento, U. (1995). An implementation of von Neumann's self-reproducing machine. *Artificial Life*, Vol. 2, No. 4, pp. 337-354
- Rietman, E. (1993). *Creating Artificial Life : Self-organizatin*. Pennsylvania : Windcrest/McGraw-Hill.



Cellular Automata - Innovative Modelling for Science and Engineering

Edited by Dr. Alejandro Salcido

ISBN 978-953-307-172-5

Hard cover, 426 pages

Publisher InTech

Published online 11, April, 2011

Published in print edition April, 2011

Modelling and simulation are disciplines of major importance for science and engineering. There is no science without models, and simulation has nowadays become a very useful tool, sometimes unavoidable, for development of both science and engineering. The main attractive feature of cellular automata is that, in spite of their conceptual simplicity which allows an easiness of implementation for computer simulation, as a detailed and complete mathematical analysis in principle, they are able to exhibit a wide variety of amazingly complex behaviour. This feature of cellular automata has attracted the researchers' attention from a wide variety of divergent fields of the exact disciplines of science and engineering, but also of the social sciences, and sometimes beyond. The collective complex behaviour of numerous systems, which emerge from the interaction of a multitude of simple individuals, is being conveniently modelled and simulated with cellular automata for very different purposes. In this book, a number of innovative applications of cellular automata models in the fields of Quantum Computing, Materials Science, Cryptography and Coding, and Robotics and Image Processing are presented.

How to reference

In order to correctly reference this scholarly work, feel free to copy and paste the following:

Sartra Wongthanavas (2011). Cellular Automata for Medical Image Processing, Cellular Automata - Innovative Modelling for Science and Engineering, Dr. Alejandro Salcido (Ed.), ISBN: 978-953-307-172-5, InTech, Available from: <http://www.intechopen.com/books/cellular-automata-innovative-modelling-for-science-and-engineering/cellular-automata-for-medical-image-processing>

INTECH
open science | open minds

InTech Europe

University Campus STeP Ri
Slavka Krautzeka 83/A
51000 Rijeka, Croatia
Phone: +385 (51) 770 447
Fax: +385 (51) 686 166
www.intechopen.com

InTech China

Unit 405, Office Block, Hotel Equatorial Shanghai
No.65, Yan An Road (West), Shanghai, 200040, China
中国上海市延安西路65号上海国际贵都大饭店办公楼405单元
Phone: +86-21-62489820
Fax: +86-21-62489821